Inorganic Chemistry

Article

pubs.acs.org/IC

Synthesis, Crystal Structure, Chemical Bonding, and Physical Properties of the Ternary Na/Mg Stannide Na_2MgSn

Takahiro Yamada,*[,†] Volker L. Deringer,[‡] Richard Dronskowski,[‡] and Hisanori Yamane[†]

[†]Institute of Multidisciplinary Research for Advanced Materials, Tohoku University, 2-1-1 Katahira, Aoba-ku, Sendai 980-8577, Japan

[‡]Institute of Inorganic Chemistry, RWTH Aachen University, Landoltweg 1, 52056 Aachen, Germany

Supporting Information

ABSTRACT: A ternary stannide of sodium and magnesium, Na_2MgSn, was synthesized from the elements, and the crystal structure was determined by single-crystal X-ray diffraction. The compound crystallizes in the Li_2CuAs structure type (hexagonal, $P6_3/mmc$, $Z = 2$, $a = 5.0486(11)$ Å, $c = 10.095(2)$ Å), and its structure is built up of two-dimensional honeycomb layers of $^2_\infty[(MgSn)^{2-}]$ stacked along the *c*-axis, with Na atoms as "space fillers". First-principles computations at various levels of density functional theory (DFT) verify that the most stable configuration is the one in which Na and Mg atoms occupy the 4*f* and 2*b* sites, respectively, and thus DFT provides a necessary complement to X-ray structural elucidation. Our computations also predict that Na_2MgSn must be a semiconductor with a small band gap. In accord with these predictions, the electrical resistivity measured for a polycrystalline sample of Na_2MgSn is 9.6−10.4 mΩ cm in the range of 90−635 K, and the Seebeck coefficient decreases from +390 μV K^{-1} (at 300 K) to +150 μV K^{-1} (at 430 K).

1. INTRODUCTION

Within the last two decades, a wide variety of alkali-metal stannides has been synthesized, and their crystal structures exhibit most diverse tin subunits and networks, ranging from zero to three in dimensionality.[1−12] In the alkali—alkaline-earth—Sn ternary systems, multiple structural fragments and networks are to be expected in the solid-state structures, because of differences in valence electron numbers and size between alkali and alkaline-earth metal cations. In the past decade, Sevov and co-workers have intensively explored such ternary phases and synthesized $Li_5Ca_7Sn_{11}$,[13] $Li_{8.84}CaSn_{6.16}$,[13] $Li_4Ba_3Sn_8$,[14] Na_8BaSn_6,[15] $Na_{10}(Ca,Sr)Sn_{12}$,[16] and Na_4CaSn_6.[17] Most compounds exhibit novel crystal structures with characteristic components, for example, aromatic pentagons of $[Sn_5]^{6-}$ (ref 13) or a large isolated cluster of $[Sn_{12}]^{12-}$ (ref 16). The ternary compounds are semiconductors with energy gaps of 0.11−4 eV, except for the highly conductive $Li_5Ba_7Sn_{11}$ and $Li_{9-x}CaSn_{6+x}$. Recently, Lei prepared two ternary compounds, $K_2Mg_{5-x}Sn_3$ and $K_3Mg_{18}Sn_{11}$ in the K−Mg−Sn system, and reported their crystal and electronic structures.[18] $K_2Mg_{5-x}Sn_3$ and $K_3Mg_{18}Sn_{11}$ contain a two-dimensional (2-D) corrugated Mg−Sn network and a three-dimensional (3-D) $[Mg_{18}Sn_{11}]$ network, respectively, and it is anticipated that both compounds are metallic.

Despite these efforts, an abundance of phases in the alkali—alkaline-earth—Sn system yet await their discovery, and such phases also promise a highly diverse structural chemistry. For example, there is no report so far on Na−Mg−Sn ternary compounds. In the present study, we report synthesis, crystal structure, and electronic as well as physical properties of Na_2MgSn, which is built up from 2-D honeycomb layers of $^2_\infty[(MgSn)^{2-}]$ with Na atoms as "space fillers".

2. EXPERIMENTAL PROCEDURES AND COMPUTATIONAL DETAILS

Synthesis. All manipulations were carried out in an argon gas-filled glovebox (MBraun, O_2, H_2O < 1 ppm), because of the air sensitivity of the reagents and samples. Sodium (lump, 99.95%, Nippon Soda Co., Ltd.), magnesium (powder, <104 μm, 99.9%, Rare Metallic Co., Ltd.), and tin (shot, 99.999%, Koujundo Kagaku Co., Ltd.) were weighed in predetermined molar ratios. A sintered BN crucible (inside diameter = 6 mm; depth = 18 mm in inner volume, Showa Denko, 99.5%) was loaded with the source elements (ca. 0.8 g in total) and sealed in a stainless steel tube (SUS316, an inner diameter of 10.5 mm, a length of 90 mm) with stainless steel caps. For the preparation of a polycrystalline bulk of Na_2MgSn, the stoichiometric amounts of the source elements were heated at 823 K for 24 h. The product was pulverized with an agate mortar and pressed into a compact (ca. 14 mm × 3 mm × 2.5 mm), which was then sintered at 913 K for 18 h in an electrical furnace. Single crystals of Na_2MgSn were obtained by heating the source elements with a molar ratio of Na:Mg:Sn = 3:1:1 at 1023 K for 3 h, followed by cooling to 873 K at a rate of −5 K/h, and subsequent cooling to room temperature in the furnace by shutting off the electric power.

Structure Elucidation. The powder X-ray diffraction (XRD) pattern of Na_2MgSn was measured under an argon atmosphere using Cu Kα radiation ($\lambda = 1.5418$ Å) with a pyrolitic graphite monochromator, a scintillation counter, and a diffractometer (Rigaku, Model RINT2200). The XRD data of a Na_2MgSn single crystal sealed in a glass capillary were collected using Mo Kα radiation with a graphite monochromator and an imaging plate on a single-crystal X-ray diffractometer (Rigaku, Model R-AXIS RAPID-II). XRD data collection and unit-cell refinement were performed by the PROCESS-AUTO program.[19] An analytical absorption correction was applied by the NUMABS program.[20] The crystal structure was refined by full-matrix least-squares on F^2 using the SHELXL-97 program.[21] All calculations were carried out on a personal computer using the WinGX

Received: January 24, 2012
Published: March 27, 2012

   dx.doi.org/10.1021/ic300184d | Inorg. Chem. 2012, 51, 4810−4816

software package.[22] The atomic coordinates were standardized by the STRUCTURE TIDY program.[23]

Electrical Properties. The electrical resistivity of the polycrystalline sample was measured in argon by a direct current four-probe method in the temperature range of 90−645 K. The Seebeck coefficient was measured in argon by a thermoelectric power (ΔE)—temperature difference (ΔT) method between 300 K and 430 K.

Quantum Chemistry. Electronic-structure computations were carried out using two different approaches: first, the all-electron scalar-relativistic Linear Muffin-Tin Orbital (LMTO) theory[24,25] in its tight-binding representation,[26] using the TB-LMTO-ASA 4.7 program,[28] and second, a plane-wave projector-augmented wave[29] approach, as implemented in the Vienna *Ab Initio* Simulation package (VASP).[30] To treat electronic exchange and correlation, the formulations by von Barth and Hedin[31] and Perdew, Burke, and Ernzerhof (PBE)[32] were used in LMTO and VASP, respectively. Experimental structures were taken as input and Na and Mg permuted where appropriate to obtain different structural models; these are described in detail below. *k*-space was sampled at points on a 16 × 16 × 8 Monkhorst−Pack grid[33] centered at the Γ point. Chemical bonding in Na_2MgSn was investigated using the Crystal Orbital Hamilton Population (COHP) technique,[34] which is an energy-resolved partitioning of the band structure energy (sum of the Kohn−Sham eigenvalues), in terms of atomic and bonding contributions.[35] As such, "off-site" COHP plots for orbital−pair interactions serve as an indicator of chemical bonding between two atoms[36] and we draw them in the conventional way: −COHP(E) is plotted such that bonding contributions fall to the right of the energy axis, and antibonding contributions to the left.

3. RESULTS AND DISCUSSION

3.1. Synthesis. Mass change was not detected after heating the elements in the BN crucible at 823 K for 24 h. The product in the crucible was powdered and pressed into a rectangular parallelepiped compact in the glovebox. A polycrystalline silver-gray bulk (13.1 mm × 2.9 mm × 2.5 mm) was obtained by heating the compact at 913 K for 18 h. A mass loss of ∼1% was observed after heating, suggesting that a trace of Na and/or Mg evaporated during the heating. The density of the sample was 2.12 g cm^{-3}, corresponding to ca. 75% of the theoretical density determined in a later section. The bulk sample was powdered for X-ray diffraction (XRD) measurement; the powder XRD pattern of the sample, measured under an argon atmosphere, is shown in Figure 1. All peaks, except a small one at 2θ = 21.4°, were indexed in the hexagonal system with unit-cell parameters of a = 5.056(5) Å, c = 10.098(8) Å. The XRD pattern is similar to that of the ternary compound Na_2CdSn,[37] which adopts the

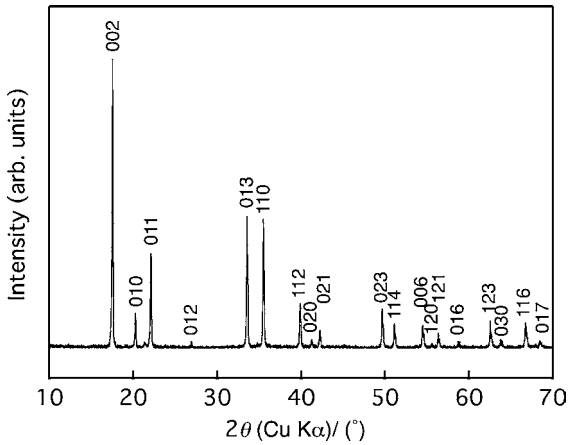

Figure 1. Powder XRD pattern of the sample prepared at 913 K for 18 h.

Li_2CuAs-type structure (hexagonal, a = 4.990 Å, c = 10.111 Å). The small unidentified peak observed at 21.4° was attributed to an impurity phase that was assumedly formed due to the evaporation of Na and/or Mg during heating. Since the amount of the impurity phase is small, judging from the XRD pattern and from the aforementioned mass loss of only 1%, the hexagonal crystalline phase is regarded to have a stoichiometric composition, namely, Na_2MgSn, in the sequel.

Flaky single crystals, silver-gray in color, with 0.03−0.20 mm in size were selected from the crushed sample prepared by heating the source elements with a molar ratio of Na:Mg:Sn = 3:1:1 at 1023 K for 3 h with subsequent slow cooling.

3.2. Crystal Structure. The single-crystal XRD reflections of Na_2MgSn were indexed with hexagonal unit-cell parameters of a = 5.0486(11) Å and c = 10.095(2) Å, which are in agreement with those of the polycrystalline sample. The observed extinction conditions were consistent with space group $P6_3/mmc$ (No. 194). The crystal structure of Na_2CdSn[37] was adopted as an initial model for structure refinement. Na rests on the Wyckoff position 4*f* ($^1/_3$, $^2/_3$, z = 0.58) of space group $P6_3/mmc$. There are reports on mixed Mg/Sn sites in the structures of some stannides,[38−40] and thus Mg/Sn mixed occupations were initially assumed for both the 2*b* (0, 0, $^1/_4$) and 2*c* ($^1/_3$, $^2/_3$, $^1/_4$) sites. The occupancy factors on the 2*b* and 2*c* sites were refined to be Mg/Sn = 1.0/0.0 and Mg/Sn = 0.0/1.0, respectively. Thus, Mg fully occupies the 2*b* site in Na_2MgSn while Sn must rest on 2*c*. Because the X-ray beam cannot distinguish Na (Z = 11) from Mg (Z = 12), the assignment of Na and Mg was later checked from electronic-structure computations (see below), and it proved to be correct. The final refinement resulted in $R1$ = 0.031 and S = 1.16 for all data, and the refined z coordinate of the Na atom was 0.5797(4). Details of the data collection and refinement are listed in Table 1. Atomic coordinates and equivalent displacement parameters (U_{eq}), as well as selected bond lengths and angles, are summarized in Tables 2 and 3.

As shown in Figures 2 and 3, Mg (2*b* site) and Sn (2*c* site) atoms lie in the same plane and form honeycomb lattice layers that stack in an ABAB sequence with an interlayer distance of 5.0475(10) Å along the *c*-axis. The atomic distance between Mg and Sn, d(Mg−Sn), in the honeycomb layer is 2.9148(3) Å and, thus, is slightly smaller than that in Mg_2Sn, adopting the anti-CaF_2 structure type with d(Mg−Sn) = 2.927 Å.[41] Ternary compounds of CaMgSn and SrMgSn[42] reported by Eisenmann et al. contain folded honeycomb lattice layers of $^2_\infty[(MgSn)^{2-}]$ within their crystal structures. The d(Mg−Sn) values in the layers of CaMgSn (2.930 and 2.931 Å) are close to the d(Mg−Sn) values we observe in Na_2MgSn, whereas the d(Mg−Sn) of 2.963 and 3.056 Å in SrMgSn are larger than those in the newly made Na_2MgSn.

Na atoms are located above and below the center of the six-membered rings of $[Mg-Sn]_3$, and the atomic arrangement of Na is similar to that of C in lonsdaleite (hexagonal diamond), as shown in Figure 2. The Na^i−Na^{ii} distance across the honeycomb layers is 3.329(3) Å, which is smaller than that of Na^{ii}−Na^{iii} (3.438(6) Å) between adjacent honeycomb lattice layers. The Na−Na interatomic distances are 6%−9% smaller than those in elemental Na.[43]

The z-coordinate of the Na atom is 0.5797(4), which slightly deviates from that (0.5816(4)) in the isostructural compound Na_2CdSn.[37] The interatomic distances d(Na^i−Na^{ii}) and d(Na^{ii}−Na^{iii}) in Na_2CdSn are 3.405(1) and 3.327(1) Å,

dx.doi.org/10.1021/ic300184d | *Inorg. Chem.* 2012, 51, 4810−4816

Table 1. Crystal Data and Refinement Results for Na_2MgSn

parameter	value
chemical formula	Na_2MgSn
formula weight, M_r	188.98 g mol^{-1}
temperature, T	293(2) K
crystal system	hexagonal
space group	$P6_3/mmc$
unit-cell dimensions	
a	5.0486(11) Å
c	10.095(2) Å
unit-cell volume, V	222.84(8) $Å^3$
Z	2
calculated density, D_{cal}	2.82 Mg m^{-3}
radiation wavelength, λ	0.71075 Å
crystal form	fragment
color	silver-gray
absorption correction	numerical
absorption coefficient, μ	5.84 mm^{-1}
crystal size	0.144 mm × 0.168 mm × 0.043 mm
limiting indices	
h	$-6 \le h \le 5$
k	$-6 \le k \le 6$
l	$-12 \le l \le 13$
F_{000}	168
θ range for data collection	4.04°−27.26°
reflections collected/unique	1796/125
R_{int}	0.030
data/restraints/parameters	125/0/8
weight parameters	
a	0.0332
b	0.2530
goodness-of-fit on F^2, S	1.16
$R1$, $wR2$ $(I > 2\sigma(I))^{a,b}$	0.0296, 0.0645
$R1$, $wR2$ (all data)^{a,b}	0.0310, 0.0655
largest diff. peak, $\Delta\rho$	0.90 e $Å^{-3}$
largest diff. hole, $\Delta\rho$	−0.45 e $Å^{-3}$

$^a R1 = \sum||F_0| - |F_c||/\sum|F_0|$. $^b wR2 = \{[\sum w[(F_0)^2 - (F_c)^2]^2]/[\sum w(F_0^2)^2]\}^{1/2}$; $w = [\sigma^2(F_0)^2 + (AP)^2 + BP]^{-1}$, where $P = [(F_0)^2 + 2(F_c)^2]/3$ and $A/B = 0.0332/0.2530$.

respectively; they are almost equal to the Na−Na distances found in Na_2MgSn.

As shown in Figure 3, Na^{ii} and Sn^{i} atoms align along the c-axis with an interatomic distance of 3.328(4) Å. The Na^{ii}−Sn distance is 3.384(2) Å and equals the shortest Na^{ii}−Mg distance. These Na−Sn distances are close to the shortest one in the binary compound NaSn (d = 3.355 Å).[4]

According to the compilation in Pearson's structural database,[44] only three ternary compounds containing the elements Na and Mg were previously known (if one ignores hydrides and halides): $Na_{2.5}Mg_{2.5}Ga_9$,[45] NaMgAs, and NaMgSb.[46] Of those compounds, $Na_{2.5}Mg_{2.5}Ga_9$ has six mixed sites occupied by Na and Mg in the crystal structure, while the two pnictides contain no mixed occupancies. The pnictides are composed of bent 2D square lattice layers of $^2_\infty[Mg(As,Sb)^-]$ stacked with Na atoms. The shortest Na−Mg distances reported for the structures of NaMgAs and NaMgSb are 3.438 Å and 3.612 Å, respectively, which are 1.6% and 6.7% larger than that of Na_2MgSn (d = 3.384(2) Å).

Summing it up, the refined solid-state structure of Na_2MgSn—in particular, regarding the interatomic distances—is consistent with the crystal structures of isostructural and other structurally related compounds. However, it is impossible to distinguish Na from Mg, which are direct

Table 3. Selected Bond Lengths and Angles in Na_2MgSn

bond pair	bond length (Å)	bond angle vertices	bond angle (°)
Na^{i}−Na^{ii}	3.438 (6)	Na^{i}−Na^{ii}−Na^{iii}	118.90 (14)
Na^{ii}−Na^{iii}	3.329 (3)	Na^{iii}−Na−Na^{iii}	98.61 (11)
Na^{i}−Mg	3.384 (2)	Na^{i}−Na^{ii}−Sn	59.47 (6)
Na^{ii}−Mg	3.384 (2)	Na^{i}−Na^{ii}−Sn^{i}	180.00
Na^{i}−Sn	3.384 (2)	Sn−Na^{ii}−Sn^{i}	120.53 (7)
Na^{ii}−Sn	3.384 (2)	Mg−Na^{ii}−Sn^{i}	120.53 (7)
Na^{ii}−Sn^{i}	3.328(4)	Mg−Na^{i}−Sn	51.02 (3)
Mg−Sn	2.9148 (3)	Mg−Na^{ii}−Sn	51.02 (3)
		Mg−Sn−Mg	120.00
		Sn−Mg−Sn	120.00

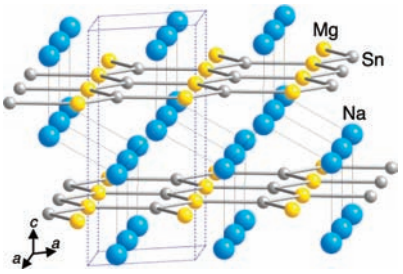

Figure 2. Schematic drawing of the crystal structure of Na_2MgSn. Na atoms are drawn in teal, Mg in yellow, and Sn in gray.

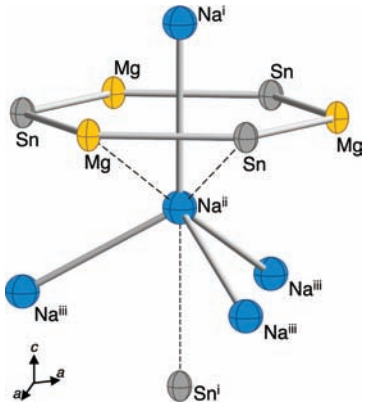

Figure 3. Atom coordination around a Na atom. Atoms are drawn as 75% probability ellipsoids. Symmetry codes: (i) $-x, -y, -z$, (ii) $-x, -y, -z + {}^1/_2$, and (iii) $x, y, -z + {}^1/_2$.

Table 2. Atomic Coordinates and Anisotropic and Isotropic Displacement Parameters.^{a}

atom	site	x	y	z	U_{11} ($Å^2$)	U_{33} ($Å^2$)	U_{12} ($Å^2$)	U_{eq} ($Å^2$)
Na	4f	1/3	2/3	0.5794(4)	0.0363(15)	0.035(2)	0.0182(7)	0.0360(10)
Mg	2b	0	0	1/4	0.0172(10)	0.0328(18)	0.0086(5)	0.0224(7)
Sn	2c	1/3	2/3	1/4	0.0185(4)	0.0293(5)	0.00927(19)	0.0221(4)

$^a U_{11} = U_{22}$, $U_{23} = U_{13} = 0$, $U_{eq} = (\sum_i \sum_j U_{ij}\, a_i{*}a_j{*}a_i{\cdot}a_j)/3$.

dx.doi.org/10.1021/ic300184d | Inorg. Chem. 2012, 51, 4810−4816

neighbors in the periodic table of the elements, by XRD experiment *alone*, because of the similar atomic scattering factors. Indeed, a refinement of the structure based on a structural model with Na/Mg mixed sites (and a restriction of the chemical composition to Na_2MgSn, of course) resulted in Na site occupancies of 58% and 16% at 4*f* and 2*b*, respectively, with $R1 = 3.0\%$ and $S = 1.17$ for all data. The reliability factors were virtually equal to those of the ordered model ($R1 = 3.1\%$, $S = 1.16$): in other words, *no definitive assessment is possible from refinement alone*. To circumvent this issue and unambiguously clarify the Na/Mg positions in the crystal, we performed a complementary, quantum-chemical investigation, which is reported in the next section.

3.3. Quantum-Chemical Computations. To verify the ordering configuration of Na and Mg in the crystal structure of Na_2MgSn, we performed theoretical computations in the framework of density-functional theory (DFT), which has become the method of choice for most solid-state quantum chemical questions.[35] Our aim is 2-fold: we seek to (1) distinguish possible distributions of Na and Mg in the crystal by evaluating the corresponding electronic energies, and (2) *understand* the electronic structure and chemical bonding in the newly synthesized compound. We chose two principally different routes, to avoid ambiguities in one particular DFT method: namely, we performed tight-binding computations with a local basis set (TB-LMTO-ASA program),[24] as well as plane-wave DFT computations (using the VASP package).[30] Local (LDA) and semilocal (GGA) approximations to the exchange-correlation functional were chosen, respectively, again to verify that our results are not exclusive to one particular method.

Regarding the structures derived from XRD, there are several possibilities of assigning Na and Mg atoms, and they are sketched in Figure 4: model (a) is a fragment cut from the proposed Li_2CuAs structure type, with only Mg in the

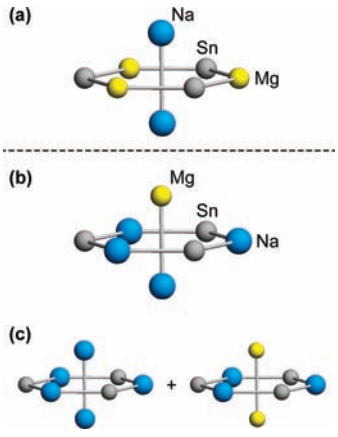

Figure 4. Motifs in the structural models for DFT computations on Na_2MgSn. Relevant fragments from the Li_2CuAs type structure ((a)) and two hypothetical structures ((b) and (c)).

honeycomb layers, and only Na between the layers; models (b) and (c) represent two models with only Na in the honeycomb layers, and the remaining Na and Mg distributed around the honeycomb layers. In these cases, the space group lowers to $P6_3/mc$ and $P3m1$, respectively. Quick single-point computations immediately verify that both models (b) and (c) with Na in the honeycomb layers may be safely discarded; the energetic cost is predicted to be 45.4−49.3 kJ mol^{-1} (LDA) or 63.0−67.1 kJ mol^{-1} (GGA), as given in Table 4; the slight differences caused by the two fundamentally different DFT

Table 4. Energy Differences for the Various Structural Models (cf Figure 4), Computed at Various Levels of Density Functional Theory[a]

		Energy			
		LMTO/LDA		VASP/GGA	
model	space group	(eV/cell)	(kJ mol^{-1})	(eV/cell)	(kJ mol^{-1})
(a)	$P6_3/mmc$	0 (ref)	0 (ref)	0 (ref)	0 (ref)
(b)	$P6_3/mc$	+0.94	+45.4	+1.30	+63.0
(c)	$P3m1$	+1.02	+49.3	+1.39	+67.1

[a]Energies are given per cell and per formula unit, respectively.

methods (local orbitals versus plane waves) are unimportant in the light of this clear energetic preference toward the Li_2CuAs type (model (a)).[47] Finally, one may think of mixed occupations in the honeycomb layer (i.e., Na and Mg sharing what was assigned as the 2*b* site). We thus set up "2 × 2 × 1" supercells (doubling the experimentally determined cell in the *a* and *b* directions) in which we randomly permuted various Na and Mg atoms, such that a certain amount of Na atoms occupied the former Mg positions in the honeycomb lattice; of course, the chemical composition of all supercells remained unchanged. The resulting VASP energies are plotted in Figure 5, and they show an almost linear increase in energy as more Na is placed into the honeycomb layers. These results safely

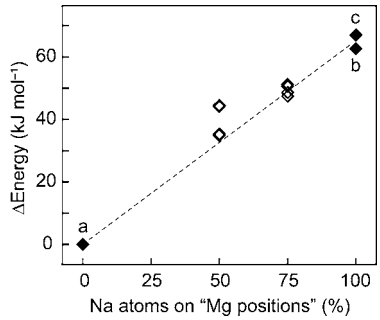

Figure 5. Dependence of the computed energies (DFT/GGA) for Na_2MgSn on the occupancy of Na atoms on the proposed Mg positions ("2*b* site"). Filled diamonds (◆) correspond to the structural models shown in Figure 4 (marked as a, b, and c), while open diamonds (◇) refer to supercell computations as described in the text. The dashed line serves only as a guide to the eye.

eliminate the possibility of Na/Mg mixed occupations in the structure. The propositions of the preceding section are thus proven correct quantum-chemically: Na_2MgSn crystallizes in the Li_2CuAs structure type.

To gain further insight into the chemical bonding, we computed the densities of states (DOS, given in states eV^{-1} cell^{-1}) as well as the crystal orbital Hamilton populations (−COHP, per bond) for the respective nearest-neighbor interactions in Na_2MgSn, and these curves are shown in Figures 6 and 7, respectively. Integrated −COHP (−ICOHP) were computed and tabulated in Table 5. The (P)DOS plots indicate two well-separated sets of bands in the valence region, namely, an area of mainly s character at −8 eV to −6.5 eV (relative to the Fermi level, ε_F), and a more p-dominated area starting at approximately −3.75 eV; this is not unexpected for

dx.doi.org/10.1021/ic300184d | Inorg. Chem. 2012, 51, 4810−4816

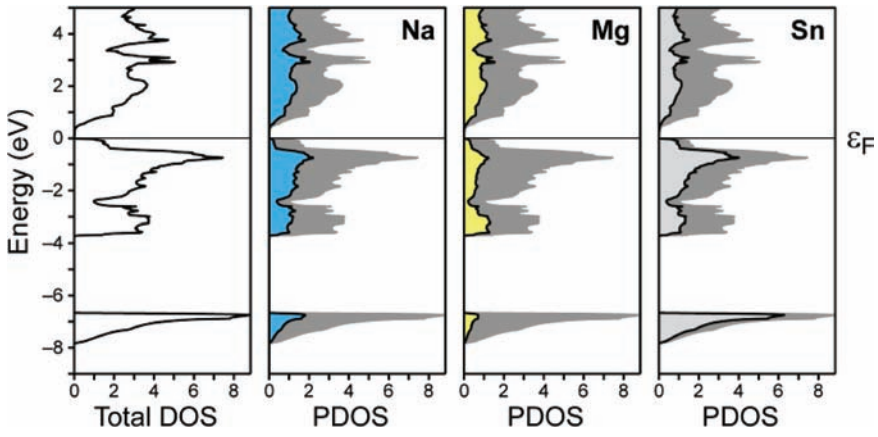

Figure 6. Total and partial densities-of-states (DOS, PDOS, respectively) of Na_2MgSn obtained from TB-LMTO-ASA computations. In the PDOS curves, the gray shaded area indicates the total DOS for comparison. A horizontal line marks the Fermi level ε_F, which has been arbitrarily set to 0 eV throughout this work.

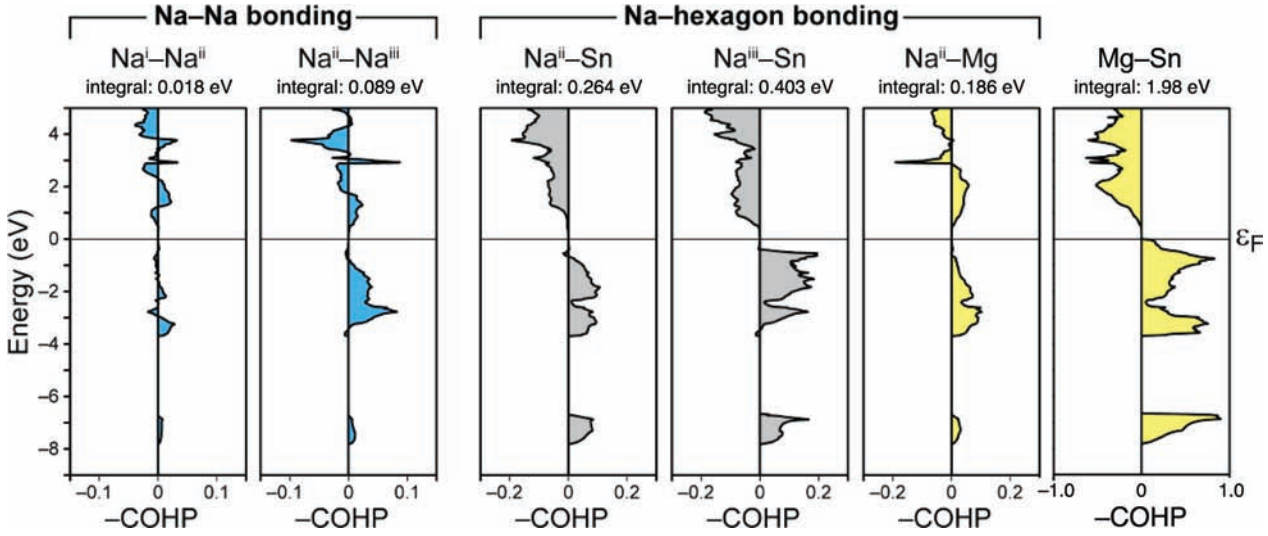

Figure 7. Selected crystal orbital Hamilton population (COHP) curves for atom-pair interactions in Na_2MgSn. Integrated −COHP values (−ICOHP) up to the Fermi level, for one bond each, are given at the head of the graphs.

Table 5. ICOHP up to the Fermi Level, Given per Bond and per Unit Cell, for Selected Bonds

bond	d (Å)	−ICOHP (eV/bond)	× N per cell	−ICOHP (eV/cell)
Na^{i}–Na^{ii}	3.438	0.018	× 2	0.036
Na^{ii}–Na^{iii}	3.329	0.089	× 6	0.534
Na^{ii}–Sn^{a}	3.384	0.264	× 12	3.168
Na^{iii}–Sn	3.329	0.403	× 4	1.612
Na^{ii}–Mg^{a}	3.384	0.186	× 12	2.232
Mg–Sn	2.915	1.98	× 6	11.88

^{a}Na^{i} and Na^{ii} are equivalent in this case.

this compound of main-group metals (additional *l*-resolved PDOS plots are provided in the Supporting Information). Furthermore, the DOS plot shows a small band gap of ~0.4 eV above the Fermi level (ε_F). It must be noted that "pure" DFT typically underestimates the size of the gap,[35] and the computational prediction rather serves as a qualitative measure; nonetheless, Na_2MgSn is clearly predicted to be a semiconductor, and this prediction will be tested, experimentally, in the next section. Looking at the chemical bonding, the top of the valence bands is dominated by Mg−Sn bonding interactions: a −COHP(E) integration up to the Fermi level gives 1.98 eV per bond or 11.88 eV per unit cell, which is, by far, the largest contribution *per bond* among those shown in Figure 7. The second largest contributions are made by Na−hexagon bonds (Na^{ii}−Sn, Na^{iii}−Sn, and Na^{ii}−Mg, respectively), out of which the covalent Na^{iii}−Sn interaction is predicted to be strongest (but still weaker by a factor of 5 than the Mg−Sn bond). The three types of Na−hexagon bonds contribute ICOHP values of 3.17, 1.61, and 2.23 eV *per unit cell*, respectively, which together constitute 36% of the ICOHPs listed in Table 5. Remarkably, the Na−Na COHP interactions shown in Figure 7 are almost nonexistent, compared to the other bonds (mind the different scales in the COHP plots); consequently, summing up over the entire unit cell, Na−Na pairs contribute a mere 3% of all ICOHP values listed in Table 5. Summarizing, Na_2MgSn can be regarded as a stacking of strongly bonded Mg−Sn honeycomb layers that are linked by less strong Na−Mg and Na−Sn interactions.

3.4. Physical Properties. The electrical resistivity (ρ) and Seebeck coefficient (S) of a polycrystalline sample of Na_2MgSn are shown in Figure 8. The ρ value is 9.6 mΩ cm at 90 K and slightly increases to a maximum of 10.4 mΩ cm at 360 K.

dx.doi.org/10.1021/ic300184d | Inorg. Chem. 2012, 51, 4810−4816

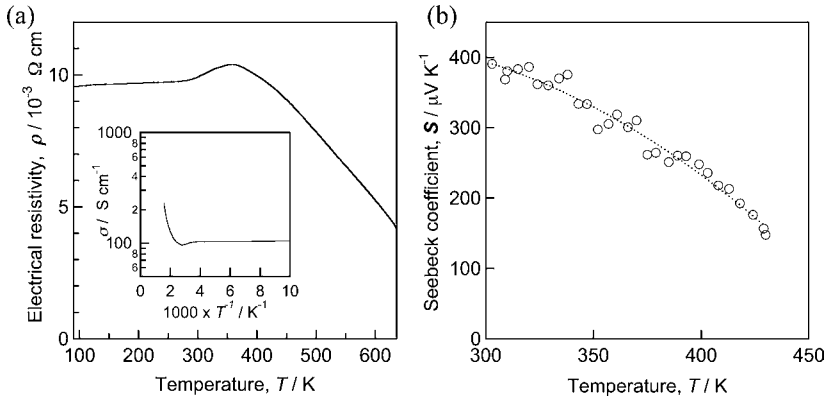

Figure 8. (a) Electrical resistivity (ρ) and (b) Seebeck coefficient (S) of the polycrystalline sample of Na_2MgSn. The inset in panel a shows the electrical conductivity of Na_2MgSn as a function of reciprocal temperature.

Beyond that, it gradually decreases with increasing temperature. Although the relative density of the Na_2MgSn sample (75%) in the present study may not be sufficient to discuss the behavior of the electrical resistivity in a quantitative way, the ρ values are 3 orders of magnitude higher than those of the constituting metals (4.8 $\mu\Omega$ cm for Na,[48] 4.4 $\mu\Omega$ cm for Mg,[49] and Sn (10 $\mu\Omega$ cm)[50] at room temperature. The inset in Figure 8a is an Arrhenius plot of the conductivity. The activation energy obtained from the linear fit in the temperature range of 570−635 K gives a value of 0.17(1) eV. These results, in accord with the DOS shown in Figure 7 (see discussion above), suggest that Na_2MgSn is not a typical metal but a narrow-gap semiconductor.

The Seebeck coefficient (S) of the polycrystalline sample is +390 μV K^{-1} at 300 K, and it monotonically decreases with increasing temperature, reaching +150 μV K^{-1} at 430 K. The positive values of S indicate that holes are the majority carriers in Na_2MgSn. The maximum thermoelectric power factor of Na_2MgSn calculated with the formula S^2/ρ amounts to 1.5 × 10^{-3} W m^{-1} K^{-2} at 300 K, ∼40% of that of Bi_2Te_3 which is one of the best thermoelectric materials known to date (ρ = 1.0 mΩ cm, S = 200 μV K^{-1}, power factor = 4 × 10^{-3} W m^{-1} K^{-2} at room temperature[51]). Further work will focus on the preparation of highly dense bulk Na_2MgSn samples showing lower electrical resistivity, as well as the characterization of its thermal conductivity.

4. CONCLUSIONS

The novel intermetallic compound disodium magnesium stannide (Na_2MgSn) was synthesized by heating stoichiometric amounts of the elements. The crystal structure of Na_2MgSn (hexagonal, $P6_3/mmc$, Z = 2, a = 5.0486(11) Å, c = 10.095(2) Å) was determined by combining X-ray single-crystal structure analysis with first-principles DFT calculations. Once more, both approaches prove to be symbiotic and *together* they provide a well-founded description of the crystal chemistry.[52] Unambiguously, they arrive at a structure based on the Li_2CuAs type with the following positions of atoms: Na on 4*f* ($^1/_3$, $^2/_3$, z) with z = 0.5816(4); Mg on 2*b* (0, 0, $^1/_4$) and Sn on 2*c* ($^1/_3$, $^2/_3$, $^1/_4$). Computed DOS and−ICOHP values suggest that the covalent Mg−Sn bonds in the 2-dimensional honeycomb-lattice layer are strongest in the structure, and the electronic properties are mainly determined by the honeycomb layers, justifying our initial dubbing of the Na atoms as "space fillers". The electrical resistivity of the polycrystalline sample of Na_2MgSn exhibits little temperature dependence in the range of 90−635 K, and the values of 9.6−10.4 mΩ cm are a few magnitudes larger than those of typical metals. The material's maximum Seebeck coefficient (S) is +390 μV K^{-1}, and the thermoelectric power factor amounts to 1.5 × 10^{-3} W m^{-1} K^{-2} at 300 K.

■ ASSOCIATED CONTENT

Supporting Information

X-ray crystallographic data in CIF format and *l*-resolved partial densities of states (PDOS) plots from TB−LMTO−ASA computations. This material is available free of charge via the Internet at http://pubs.acs.org.

■ AUTHOR INFORMATION

Corresponding Author

*Tel./Fax: +81-22-217-5813. E-mail: yamataka@tagen.tohoku.ac.jp.

Notes

The authors declare no competing financial interest.

■ ACKNOWLEDGMENTS

The authors thank Prof. U. Englert of RWTH Aachen University for helpful comments on the structural analysis. This work was supported in part by a Grant-in-Aid for Scientific Research (C) (23550222) from the Ministry of Education, Culture, Sports, Science and Technology of Japan. VLD gratefully acknowledges a scholarship from the German National Academic Foundation.

■ REFERENCES

(1) (a) Fässler, T. F. *Z. Anorg. Allg. Chem.* **2006**, *632*, 1125−1129. (b) Scharfe, S.; Kraus, F.; Stegmaier, S.; Schier, A.; Fässler, T. F. *Angew. Chem., Int. Ed.* **2011**, *50*, 3630−3670.

(2) Ienco, A.; Hoffmann, R.; Papoian, G. *J. Am. Chem. Soc.* **2001**, *123*, 2317−2325.

(3) Fortner, J.; Saboungi, M. L.; Enderby, J. E. *Phys. Rev. Lett.* **1995**, *74*, 1415−1418.

(4) Grin, Y.; Baitinger, M.; Kniep, R.; von Schnering, H. G. *Z. Kristallogr., New Cryst. Struct.* **1999**, *214*, 453−454.

(5) Baitinger, M.; Grin, Y.; Kniep, R.; von Schnering, H. G. *Z. Kristallogr., New Cryst. Struct.* **1999**, *214*, 457−458.

(6) Haarmann, F.; Grüner, D.; Bezugly, V.; Rosner, H.; Grin, Y. *Z. Anorg. Allg. Chem.* **2006**, *632*, 1423−1431.

(7) Fässler, T. F.; Hoffmann, S. *Inorg. Chem.* **2003**, *42*, 5474−5476.

(8) Dubois, F.; Schreyer, M.; Fässler, T. F. *Inorg. Chem.* **2005**, *44*, 477−479.

(9) Vaughey, J. T.; Corbett, J. D. *Inorg. Chem.* **1977**, *36*, 4316−4320.

(10) Fässler, T. F.; Kronseder, C. *Angew. Chem., Int. Ed.* **1998**, *37*, 1571−1575.
(11) Zhao, J. T.; Corbett, J. D. *Inorg. Chem.* **1994**, *33*, 5721−5726.
(12) Nolas, G. S.; Chakoumakos, B. C.; Mahieu, B.; Long, G. J.; Weakley, T. J. R. *Chem. Mater.* **2000**, *12*, 1947−1953.
(13) Todorov, I.; Sevov, S. C. *Inorg. Chem.* **2005**, *44*, 5361−5369.
(14) Bobev, S.; Sevov, S. C. *J. Alloys Compd.* **2002**, *338*, 87−92.
(15) Todorov, I.; Sevov, S. C. *Inorg. Chem.* **2004**, *43*, 6490−6494.
(16) Bobev, S.; Sevov, S. C. *Inorg. Chem.* **2001**, *40*, 5361−5364.
(17) Todorov, I.; Sevov, S. C. *Inorg. Chem.* **2006**, *45*, 4478−4483.
(18) Lei, X. W. *J. Solid State Chem.* **2011**, *184*, 852−858.
(19) *PROCESS-AUTO*; Rigaku/MSC & Rigaku Corporation: The Woodlands, TX, USA and Akishima, Tokyo, Japan, 2005.
(20) Higashi, T. *NUMABS-Numerical Absorption Correction*; Rigaku Corporation: Tokyo, 1999.
(21) Sheldrick, G. M. *Acta Crystallogr. Sect. A: Found. Crystallogr.* **2008**, *64*, 112−122.
(22) Farrugia, L. J. *J. Appl. Crystallogr.* **1999**, *32*, 837−838.
(23) Gelato, L. M.; Parthé, E. *J. Appl. Crystallogr.* **1987**, *20*, 139−143.
(24) Andersen, O. K. *Phys. Rev. B* **1975**, *12*, 3060−3083.
(25) Andersen, O. K. In *The Electronic Structure of Complex Systems*; Phariseau, P., Temmerman, W. M., Eds.; Plenum Press: New York, 1984.
(26) Andersen, O. K.; Jepsen, O. *Phys. Rev. Lett.* **1984**, *53*, 2571−2574.
(27) Krier, G.; Jepsen, O.; Burkhardt, A.; Andersen, O. K. The TB-LMTO-ASA program, version 4.7; Max-Planck-Institut Festkörperforschung: Stuttgart, Germany.
(28) For TB-LMTO-ASA computations, the downfolding technique by Lambrecht and Andersen was applied for the Na 3p states, as well as for all d and f partial waves: Lambrecht, W. R. L.; Andersen, O. K. *Phys. Rev. B* **1986**, *34*, 2439−2449. The minimal basis considered for the bonding analysis thus comprises Na 3s, Mg 3s 3p, Sn 5s 5p.
(29) Blöchl, P. E. *Phys. Rev. B* **1994**, *50*, 17953−17979.
(30) (a) Kresse, G.; Hafner, J. *Phys. Rev. B* **1993**, *47*, 558−561. (b) Kresse, G.; Furthmüller, F. *Comput. Mater. Sci.* **1996**, *6*, 15−50. (c) Kresse, G.; Joubert, D. *Phys. Rev. B* **1999**, *59*, 1758−1775.
(31) von Barth, U.; Hedin, L. *J. Phys. C: Solid State Phys.* **1972**, *5*, 1629−1642.
(32) Perdew, J. P.; Burke, K.; Ernzerhof, M. *Phys. Rev. Lett.* **1996**, *77*, 3865−3868.
(33) Monkhorst, H. J.; Pack, J. D. *Phys Rev. B* **1976**, *13*, 5188−5192.
(34) Dronskowski, R.; Blöchl, P. E. *J. Phys. Chem.* **1993**, *97*, 8617−8624.
(35) Dronskowski, R. *Computational Chemistry of Solid State Materials*; Wiley−VCH: Weinheim, Germany, 2005.
(36) A beautiful review of the concepts behind such energy-partitioning visual bonding indicators is given in: Hoffmann, R. *Angew. Chem., Int. Ed. Engl.* **1987**, *26*, 846−878.
(37) Matthes, R.; Schuster, H. U. *Z. Naturforsch. B* **1980**, *35*, 778−780.
(38) Schlüter, M.; Kunst, A.; Pöttgen, R. *Z. Anorg. Allg. Chem.* **2002**, *628*, 2641−2646.
(39) Schlüter, M.; Häussermann, U.; Heying, B.; Pöttgen, R. *J. Solid State Chem.* **2003**, *173*, 418−424.
(40) Hlukhyy, V.; Rodewald, U. Ch.; Pöttgen, R. *Z. Anorg. Allg. Chem.* **2005**, *631*, 2997−3001.
(41) Grosch, G. H.; Range, K. J. *J. Alloys Compd.* **1996**, *235*, 250−255.
(42) Eisenmann, B.; Schäfer, H.; Weiss, A. *Z. Anorg. Allg. Chem.* **1972**, *391*, 241−254.
(43) Kanda, F. A.; Stevens, R. M.; Keller, D. V. *J. Phys. Chem.* **1965**, *69*, 3867−3872.
(44) Villars, P.; Cenzual, K. *Pearson's Crystal Data*, Release 2010/11; ASM International: Materials Park, OH, USA.
(45) Nesper, R. *Angew. Chem., Int. Ed. Engl.* **1989**, *28*, 58−59.
(46) Kernkel, B.; Schuster, H. U. *Z. Naturforsch. B* **1978**, *33*, 1080−1082.
(47) Of course, one might also perform TB−LMTO−ASA computations using a GGA formulation, and/or VASP computations with LDA pseudo-potentials for completeness. In fact, we did the former, and found that the ICOHP values reported in Table 5 do not change noticeably. As discussed in the text, we only seek to rule out the presence of Na in the layer, and so the additional data have been omitted for conciseness.
(48) Bradshaw, F. J.; Pearson, S. *Proc. Phys. Soc. B* **1956**, *69*, 441−448.
(49) Chi, T. C. *J. Phys. Chem. Ref. Data* **1979**, *8*, 439−497.
(50) Chuah, D. G. S.; Ratnalingam, R.; Seward, R. J. *J. Low Temp. Phys.* **1978**, *31*, 153−173.
(51) Scherrer, H., Scherre, S., Rowe, D. M., Eds.; *CRC Handbook of Thermoelectrics*; CRC Press: Boca Raton, FL, 1995; p 211.
(52) Hoepfner, V.; Dronskowski, R. *Inorg. Chem.* **2011**, *50*, 3799−3803.